NUCL SCI TECH (2018) 29:50
https://doi.org/10.1007/s41365-018-0383-3

Novel method to measure unloaded quality factor of resonant cavities at room temperature

Ping Wang[1,2] · Jia-Ru Shi[1,2] · Zheng-Feng Xiong[3] · Ze-Ning Liu[1,2] · Cheng Cheng[1,2] · Huai-Bi Chen[1,2]

Received: 14 May 2017 / Revised: 24 July 2017 / Accepted: 4 September 2017 / Published online: 13 March 2018

Abstract We demonstrated a novel method to measure the unloaded quality factor (Q factor) of high-Q resonant cavities. This method was used to obtain data with low errors and calculate the unloaded Q factor. This procedure was more reliable than traditional methods. The data required for the method were near the resonant frequency, not at the half-power points of the reflection coefficient curve or Smith chart. We applied the new method to measure a resonant cavity with an unloaded Q factor of $\sim$ 100,000, obtaining good agreement between the measured and theoretical results.

Keywords Resonant cavity · Q factor · LRC circuit · Coupling coefficient

1 Introduction

Resonant cavities have many applications in accelerator fields, such as pulse compressors [1, 2], standing wave deflectors [3, 4], and standing wave linacs [5, 6]. In these structures, the resonant cavities are all one-port devices. The unloaded quality factor (unloaded Q factor), coupling coefficient, and resonant frequency are the main parameters. In particular, the unloaded Q factor can be used to predict the performance of the structures. In linacs and deflectors, the unloaded Q factor and input power can be used to estimate the field in the structures. In pulse compressors, the Q factor and coupling coefficient determine the peak power of the output pulse and efficiency of the system [1].

Tsinghua University has conducted research on radio frequency (RF) pulse compressors, wherein high-Q factor resonant cavities are key parts in storing the energy of an input RF pulse. Precise measurement of the Q factor of resonant cavities is necessary before powering them with a high-powered microwave. Many methods, such as energy decay in the cavity, the Smith chart, and reflection coefficient, can be utilized to measure the unloaded Q factor of a resonant cavity with one port [7–14]. In the decay method, the power leaving a resonant cavity decreases exponentially and is measured to determine the Q factor [14]. In the Smith chart and reflection coefficient methods, the unloaded quality factor can be obtained by measuring the half-power points on the Smith chart or the reflection and coupling coefficients of the resonant cavity [15, 16]. For devices with two ports, the Q factor can be derived from the transmission coefficient data [17–20].

The Smith chart and reflection coefficient of a resonant cavity can be measured using a vector network analyzer (VNA) that is used to characterize passive and active devices by measuring their network parameters, called scatter parameters (S-parameters), as functions of frequency. Using VNA enables the Smith chart reflection

This work was supported by the National Key Research and Development Program of China (No. 2016YFA0401902).

✉ Ping Wang
ping-wang13@mails.tsinghua.edu.cn

1 Department of Engineering Physics, Tsinghua University, Beijing 100084, China

2 Key Laboratory of Particle and Radiation Imaging of Ministry of Education, Tsinghua University, Beijing 100084, China

3 Northwest Institute of Nuclear Technology, Xi'an 710024, China

coefficient methods to be the two common methods for measuring the Q factor of a one-port resonant cavity.

Many factors influence the measurements of the Smith chart and reflection coefficient through VNA. One of the factors is VNA calibration that reduces systematic errors and corrects the imperfections of cables and connectors [21]. Other factors include the ambient temperature and mechanical vibration from the measurement circumstances. The noises from these factors influence the half-power points in the Smith chart and reflection coefficient curves and may lead to significant errors when measuring the unloaded Q factor.

We demonstrated a new method to measure the unloaded Q factor of resonant cavities for pulse compressors. The method is based on the reflection-type measurement by VNA. The data required to calculate the Q factor are near the resonant frequency of the reflection coefficient curve.

2 Equivalent circuit model

An equivalent model of a parallel resonant circuit driven by a current consists of a RF-resonant cavity coupled with the waveguide, as shown in Fig. 1. In this model, the resonant cavity consists of inductance (L), capacitance (C), and circuit shunt resistance (R). This resonant cavity couples with the waveguide through a coupler, which is the transformer in the equivalent model.

From the circuit model, the impedance of the resonant cavity is [15]

$$Z_c = \frac{\beta Z_0}{1 + jQ_0\left(\frac{f}{f_0} - \frac{f_0}{f}\right)}. \tag{1}$$

In Eq. (1), Z_0 is the characteristic impedance of the input transfer line and Q_0 is the unloaded Q factor given by:

$$Q_0 = 2\pi f_0 RC, \tag{2}$$

where f_0 is the resonance frequency. The coupling coefficient is defined as

$$\beta = \frac{R}{n^2 Z_0} = \frac{Q_0}{Q_e}, \tag{3}$$

where Q_e is the external Q factor.

The input reflection coefficient, which can be directly measured by VNA, is

$$\Gamma = \frac{Z_c - Z_0}{Z_c + Z_0}. \tag{4}$$

We can rewrite the reflection coefficient from the previous relations as follows

$$\Gamma = \frac{(\beta - 1) - jQ_0\xi}{(\beta + 1) + jQ_0\xi}, \tag{5}$$

where $\xi = \omega/\omega_0 - \omega_0/\omega$. The reflection curve and Smith chart with different coupling coefficients and the same unloaded Q factors are shown in Fig. 2.

Equation (5) can be rewritten as

$$\xi^2 - \frac{1}{Q_0^2}\frac{4\beta}{1 - |\Gamma|^2} + \left(\frac{\beta + 1}{Q_0}\right)^2 = 0. \tag{6}$$

We define:

$$y = \xi^2, \tag{7}$$

$$x = \frac{4}{1 - |\Gamma|^2}, \tag{8}$$

$$a = \frac{1}{Q_0} \cdot \frac{1}{Q_e}, \tag{9}$$

$$b = \frac{1}{Q_0} + \frac{1}{Q_e}, \tag{10}$$

where a and b are dimensionless. Then, Eq. (6) becomes

$$y = ax - b^2. \tag{11}$$

In Eq. (6) the values of ξ and Γ are obtained by measuring the resonant cavity, so x and y in Eq. (7) are obtained from measurement. Equation (11) represents a line, and the quantities a and b are the slope and intercept of the line, respectively. After obtaining a and b, Q_0 and β can be calculated as follows

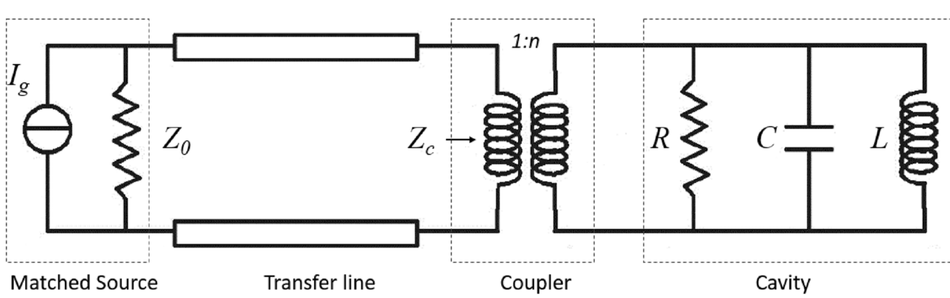

Fig. 1 Equivalent circuit of a resonant cavity coupled with a waveguide

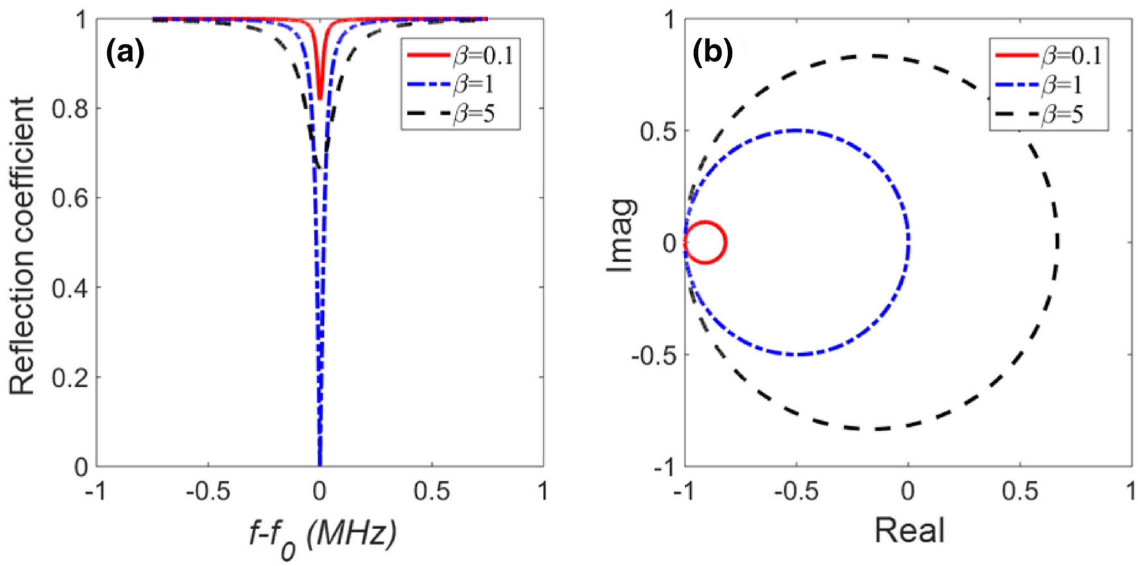

Fig. 2 (Color online) Reflection coefficient at the input port with Q_0 = 6000 for three different coupling coefficients: **a** reflection coefficient curve and **b** Smith chart

$$\begin{cases} Q_0 = \dfrac{2}{b - \sqrt{b^2 - 4a}} \\ \beta = \dfrac{b + \sqrt{b^2 - 4a}}{b - \sqrt{b^2 - 4a}} \end{cases} (\beta > 1), \tag{12}$$

$$\begin{cases} Q_0 = \dfrac{2}{b + \sqrt{b^2 - 4a}} \\ \beta = \dfrac{b - \sqrt{b^2 - 4a}}{b + \sqrt{b^2 - 4a}} \end{cases} (\beta < 1). \tag{13}$$

3 Error analysis of the measurement

Two kinds of errors may occur when performing the measurements. One is the systematic error (δ_s) that exists even after instrument calibration. The other is the noise from the measurement circumstances. The quantities directly obtained from the measurements were the frequency and reflection coefficient. Figure 3 shows the measurement scheme. The directional couplers 1 (DC1) and 2 (DC2) were used to sample the incident and reflected signals, respectively. Then, the sampled signals were downconverted to signals at low frequencies. After the analog-to-digital conversion, the digital signals were processed by the computer to obtain a_1 and b_1. The reflection coefficient of the resonant cavity was derived from the ratio of b_1 and a_1, as follows

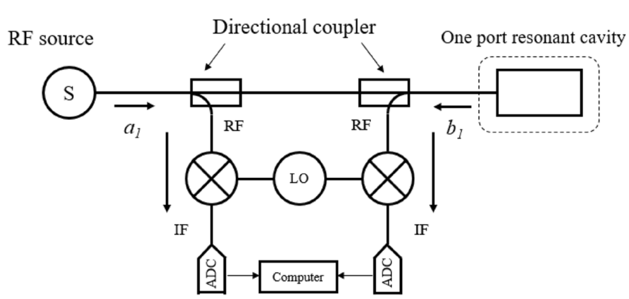

Fig. 3 Scheme of the measurement of high-Q cavity. The RF signals a_1 and b_1 were sampled by directional couplers and then downconverted to intermediate frequency (IF)

$$\Gamma = \frac{b_1}{a_1}. \tag{14}$$

The reflection coefficient with noise error is

$$\Gamma = \frac{b_1}{a_1} + \delta_n. \tag{15}$$

The noise error of the reflection coefficient is

$$\delta_n = \frac{b_1 + \delta_{b_1}}{a_1 + \delta_{a_1}} - \frac{b_1}{a_1} \tag{16}$$

where δ_{a_1} and δ_{b_1} are the errors of a_1 and b_1 and are less than a_1.

Equation (16) can be rewritten as three terms as follows

$$\delta_n = \frac{\delta_{b_1}}{a_1} - \frac{b_1}{a_1} \cdot \frac{\delta_{a_1}}{a_1} - \frac{\delta_{a_1}}{a_1} \cdot \frac{\delta_{b_1}}{a_1}. \tag{17}$$

The third term is the product of two small values and is negligible. The first and second terms are the errors contributed by the errors of a_1 and b_1. Typically, the second term is related to the value of b_1. Moreover, a small b_1 implies a small error. At the resonant frequency, the amplitude of the reflection coefficient and b_1 were the minimum values. Therefore, the error of the reflection coefficient was minimal near the resonant frequency. After including the systematic error, the reflection coefficient with errors can be written as

$$\Gamma = \frac{b_1}{a_1} + \delta_n + \delta_s. \qquad (18)$$

Figure 4 shows the influence of the systematic error. In Eq. (11), x and y represent a linear relation without errors. The systematic error destroys the linearity resulting in an x and y of the quadratic curve. The noise error was a random number with a small value. Figure 5 shows how the noise error affected the relationship of x and y. Without the noise error, x and y form a line or a quadratic curve. When the noise error was added, a simple curve cannot be used to represent x and y. The data with errors deviated from the curve without the noise error. A large noise error implied that the data deviated from the curve. Even the systematic and noise errors destroyed the linearity of x and y, and the linearity existed for small x values. From Eq. (8) and the reflection coefficient curve of a resonant cavity, the value of x near the resonant frequency was small. This condition implies that the data obtained near the resonant frequency contained minimal errors.

4 High-Q cavity and experimental setup

The geometry of the resonant cavity used in the SLED pulse compressor at Tsinghua University is a cylinder. The operation mode of the resonant cavity is TE_{015} with a low loss feature. The ratio of diameter d, to length l, of the resonant cavity was selected to maximize the frequency separation from other modes. The cavity coupled with the waveguide through two coupling holes. Using two coupling holes can reduce the effect of the TM_{115} mode in the resonant cavity. Changing the hole diameters can be used to tune the coupling coefficient of the cavity. The E and H fields of the resonant cavity are shown in Figs. 6 and 7. The electric and magnetic fields on the cylindrical surface

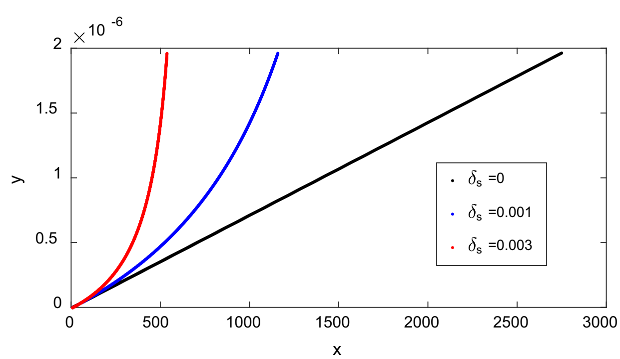

Fig. 4 (Color online) Relationship of x and y without noise errors and with different systematic errors

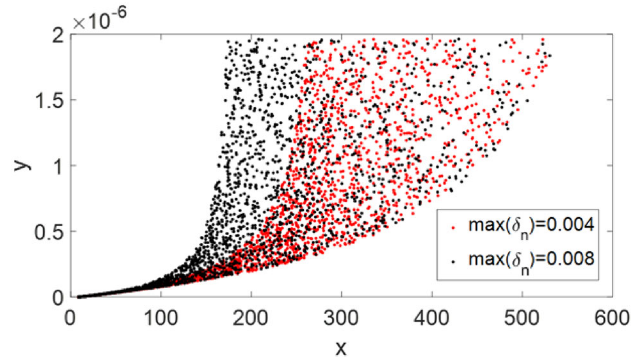

Fig. 5 (Color online) Relationship of x and y with a fixed systematic error of 0.003 and different noise errors

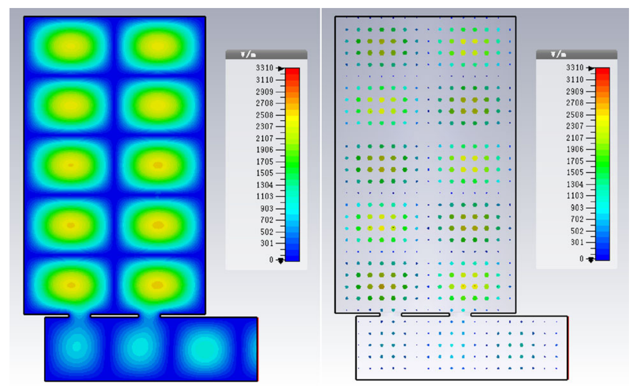

Fig. 6 (Color online) E field of high-Q cavity

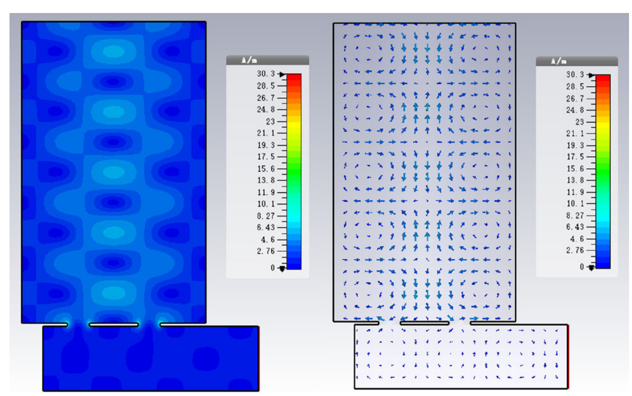

Fig. 7 (Color online) H field of high-Q cavity

were both minuscule compared with those inside the cylinder. From the computer simulation technology (CST) simulation, the unloaded Q factor of the resonant cavity without coupling holes was 108,789. Moreover, the resonant frequency was 2857.05 MHz. After adding coupling holes and the waveguide to the resonant cavity, the frequency was only minimally changed to 2855.74 MHz. The unloaded Q factor was 105,273, slightly smaller than that without coupling holes. The coupling coefficient was then tuned to 6.72.

The cavity was made of copper, and the mechanical drawings are shown in Fig. 8. The cylinder was between two copper plates with a waveguide attached to one of them and an SLAC-type flange.

Figure 9 shows the experimental setup. The measurement was taken using VNA that generated, measured, and processed the RF signals at high speed. The cavity was connected to the VNA from a microwave coaxial cable and coaxial waveguide adapter, with frequency responses calibrated for precise measurement. The VNA was fully calibrated with a short open and matched before the measurement of the reflection coefficient. In the measurement, the start and stop frequencies were set to 2853.7 and 2857.74 MHz, respectively. The number was 2001 within a span of 4 MHz. The frequency difference between two nearby points was 2 kHz. Therefore, the error of frequency measurement was less than 2 kHz that was ignored, compared with the 2.8577 GHz frequency of the cavity.

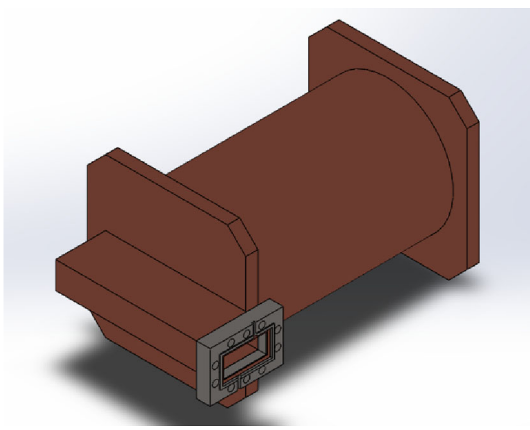

Fig. 8 (Color online) High-Q cavity assembled with the waveguide. The resonant cavities had radii of 102.55 mm and heights of 335.7 mm

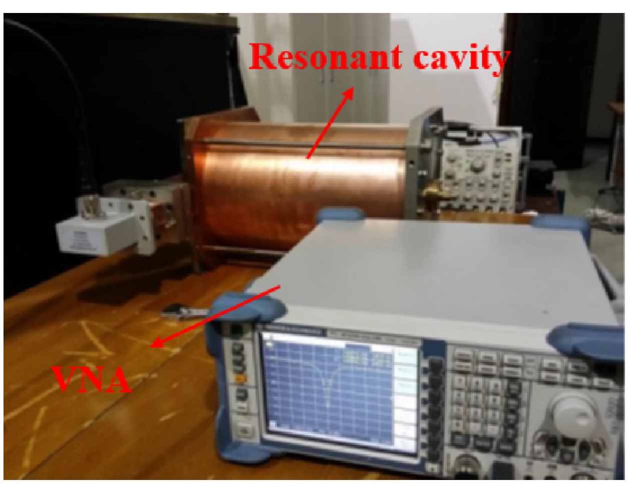

Fig. 9 (Color online) Experimental setup with the high-Q resonant cavity and a VNA

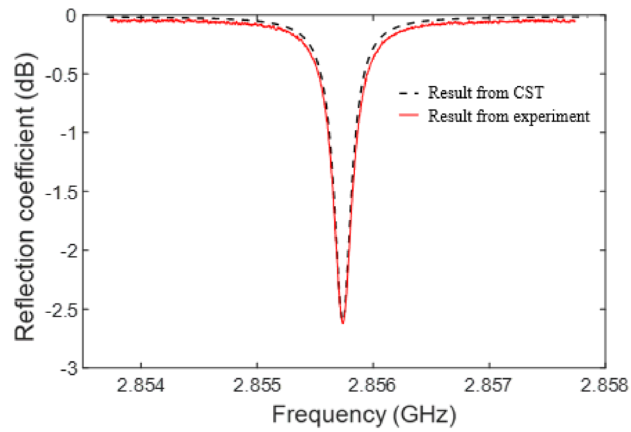

Fig. 10 (Color online) Results from CST and the experiment

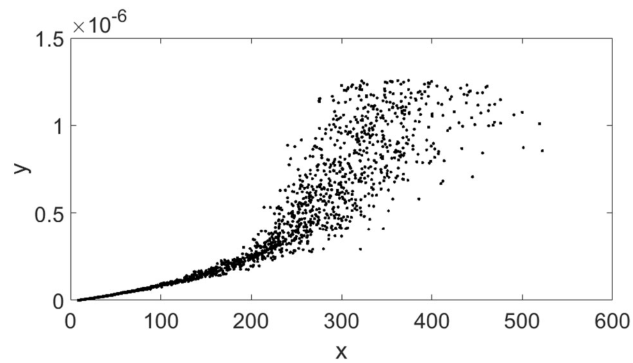

Fig. 11 Graph of x and y from the experimental data

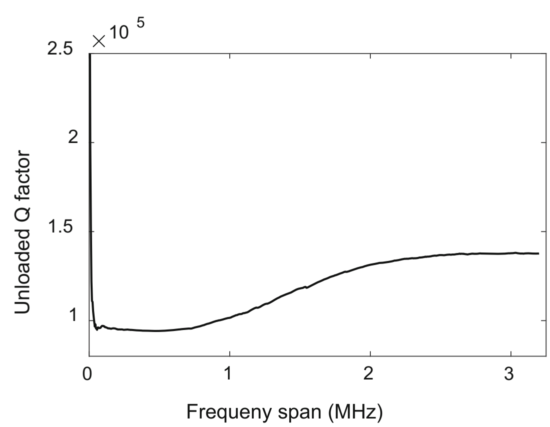

Fig. 12 Unloaded Q factor with different frequency spans

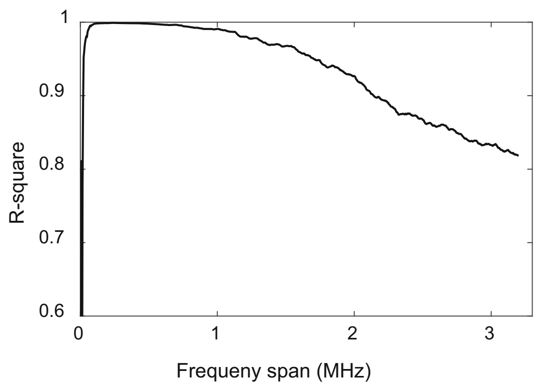

Fig. 13 *R*-square values with different frequency spans

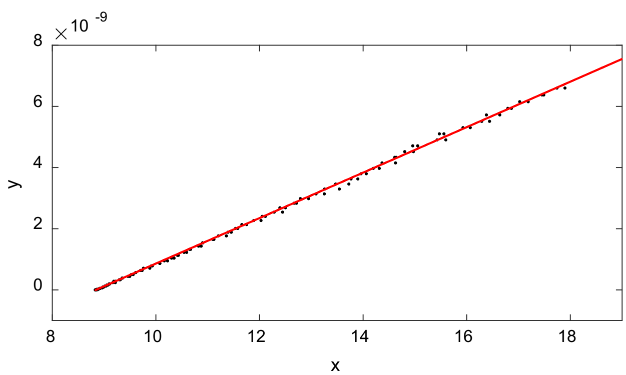

Fig. 14 (Color online) Graph of x and y with the span of best *R*-square value

Table 1 Unloaded Q factors of the resonant cavity from the simulation and experiments

Simulation from CST	105,273
Experiment with reflection coefficient method	98,166 ± 2000
Experiment with new method	96,300 ± 200

5 Results and discussion

The reflection coefficients of the resonant cavity from the simulation and measurement are shown in Fig. 10. The results were very similar.

The experimental results of Fig. 10 are represented as a graph of x and y in Fig. 11. The distribution of the points in Fig. 11 is similar to that in Fig. 5. This finding indicates that the measurements contained both systematic and noise errors. The systemic and noise errors of the reflection coefficient were estimated by overlapping the experimental and simulation results with the systemic and noise errors. Using this method, the systemic error was in the range 0.0022–0.0026 and noise error amplitude between 0.0039 and 0.0041 in this case. The error of the reflection coefficient led to the error of the unloaded quality factor of approximately ± 200, with the systemic error included in the calculation.

To minimize the noise error, the data near the resonant frequency were selected. A line was fitted to the x and y data. The goodness of the fit was evaluated by the *R*-square:

$$R\text{ - square} = \frac{\sum (\hat{y} - \bar{y})^2}{\sum (y - \bar{y})^2}, \tag{19}$$

where $\hat{y}$ is obtained from the fitting line and $\bar{y}$ is the mean value of y. Figure 12 shows the unloaded Q factor of the frequency span. When the span was small, the data used to fit a line were limited. In this case, the calculated unloaded Q factor was larger than that obtained in the simulation. Moreover, the *R*-square values of the x and y lines were less than 1 in Fig. 13. This result indicated that the linearity was poor when the span was small. When the span was between 0.224 and 0.292 MHz, the *R*-square values for x and y were greater than 0.999, indicating good linearity in this region. Therefore, the span was sufficient to fit a line. Figure 14 shows the lines of x and y with the largest *R*-square value of 0.9991774. Table 1 summarizes the results from the simulation and experiments.

6 Conclusion

A novel method was demonstrated to measure the unloaded Q factor of high-Q resonant cavities. This method can efficiently eliminate data with large errors. The frequency span with useful data should be small but large enough to fit a line. We obtained good agreement between the measured and theoretical results. This method is useful for measuring a low unloaded Q factor.

References

1. C.P. Wang, W.C. Fang, D.C. Tong et al., Design and study of a C-band pulse compressor for the SXFEL linac. Nucl. Sci. Tech. **25**, 020101 (2014). https://doi.org/10.13538/j.1001-8042/nst.25.020101
2. M. Franzi, J.W. Wang, V. Dolgashev et al., Compact rf polarizer and its application to pulse compression systems. Phys. Rev. Accel. Beams **19**, 062002 (2016). https://doi.org/10.1103/PhysRevAccelBeams.19.062002
3. Y. Nishimura, K. Sakaue, M. Nishiyama et al., Design of a two-cell rf-deflector cavity for ultra-short electron bunch measurement. Nucl. Instrum. Methods A **764**, 291–298 (2014). https://doi.org/10.1016/j.nima.2014.07.035
4. X. P. Jiang, J. R. Shi, P. Wang et al., C-band deflecting cavity for bunch length measurement of 2.5 MeV electron beam, in *Proceedings of 7th International Particle Accelerator Conference (IPAC)*, Busan, Korea, May 2016, pp. 386–388

5. L. Auditore, R.C. Barna, D. De Pasquale et al., Pulsed 5 MeV standing wave electron linac for radiation processing. Phys. Rev. Accel. Beams **7**, 030101 (2004). https://doi.org/10.1103/PhysRevSTAB.7.030101
6. L. Zhang, J.R. Shi, P. Wang et al., An X-band linac with tunable beam energy, in *Proceedings of 6th International Particle Accelerator Conference (IPAC)*, Richmond, US, May 2015, pp. 1644–1646
7. S. Shahid, J.A.R. Ball, C.G. Wells et al., Reflection type Q-factor measurement using standard least squares methods. IET Microw. Antennas Propag. **11**, 426–432 (2011). https://doi.org/10.1049/iet-map.2010.0395
8. A.J. Canós, J.M. Catalá-Civera, F.L. Peñaranda-Foix et al., A novel technique for deembedding the unloaded resonance frequency from measurements of microwave cavities. IEEE Trans. Microw. Theory Tech. **54**, 3407–3416 (2006). https://doi.org/10.1109/tmtt.2006.877833
9. P. Wang, L.H. Chua, D. Mirshekar-Syahkal, Accurate characterization of low-Q microwave resonator using critical-points method. IEEE Trans. Microw. Theory Tech. **53**, 349–353 (2005). https://doi.org/10.1109/TMTT.2004.839931
10. J.M. Drozd, W.T. Joines, Determining Q using S parameter data. IEEE Trans. Microw. Theory Tech. **44**, 2123–2127 (1996). https://doi.org/10.1109/22.543972
11. D. Kajfez, Linear fractional curve fitting for measurement of high Q factors. IEEE Trans. Microw. Theory Tech. **42**, 1149–1153 (1994). https://doi.org/10.1109/22.299749
12. D. Kajfez, Q-factor measurement with a scalar network analyser. Proc. Inst. Elect. Eng. Microw. Antennas Propag. **142**, 369–372 (1995). https://doi.org/10.1049/ip-map:19952142
13. E.-Y. Sun, S.-H. Chao, Unloaded Q measurement—the critical points method. IEEE Trans. Microw. Theory Tech. **43**, 1983–1986 (1995). https://doi.org/10.1109/22.402290
14. Y.Z. Wang, Y. Xie, T.L. Zhang et al., Quality factor measurement for MEMS resonator using time domain amplitude decaying method. Microsyst. Technol. **21**, 825–829 (2015). https://doi.org/10.1007/s00542-014-2161-4
15. D. Alesini, in *Proceedings of the CAS–CERN Accelerator School: RF for accelerators*, ed. by R. Bailey, Ebeltoft, Denmark, 8–17 June 2010, edited by, CERN-2011-007, pp. 95–116, 125–147
16. J.R. Bray, L. Roy, Measuring the unloaded, loaded, and external quality factors of one- and two-port resonators using scattering-parameter magnitudes at fractional power levels. Microw. Antennas Propag. IEE Proc. **151**, 345–350 (2004). https://doi.org/10.1002/mop.29716
17. P.J. Petersan, S.M. Anlage, Measurement of resonant frequency and quality factor of microwave resonators: comparison of methods. Appl. Phys. **84**, 3392–3402 (1998). https://doi.org/10.1063/1.368498
18. K.D. McKinstry, C.E. Patton, Methods for determination of microwave cavity quality factors from equivalent electronic circuit models. Rev. Sci. Instrum. **60**, 439–443 (1989). https://doi.org/10.1063/1.1140397
19. D.-H. Han, Y.-S. Kim, M. Kwon, Two port cavity Q measurement using scattering parameters. Rev. Sci. Instrum. **67**, 2179–2181 (1996). https://doi.org/10.1063/1.1147034
20. W. Xu, S. Belomestnykh, I. Ben-Zvi et al., Improvement of the Q-factor measurement in RF cavities, in *Proceedings of 4th International Particle Accelerator Conference (IPAC)*, Shanghai, China, May 2013, pp. 2489–2491
21. D. Kajfez, Random and systematic uncertainties of reflection-type Q-factor measurement with network analyzer. IEEE Trans. Microw. Theory Tech. **51**, 512–519 (2003). https://doi.org/10.1109/TMTT.2002.807831